ISSN 2663-1563 Vol. 5, Issue 2: 1-9, DOI: 10.25236/AJAGE.2023.050201

Investigation of the Acoustic Emission Behavior and Crack Evolution Characteristics of Limestone Broken by Static Crushing Agent

Zongwang Wu[1,3], Hongbiao Yu[2], Weiyang Cao[2], Zhaoyan Huang[1,3], Qixing Wu[1,3,*]

[1]School of Mechanics and Construction Engineering, Jinan University, Guangzhou, China
[2]CCCC Tunnel Engineering Bureau Co., Ltd., Beijing, China
[3]Key Laboratory of Major Engineering Disaster and Control, Jinan University, Guangzhou, China
wqx510632@126.com
**Corresponding author*

Abstract: *In order to investigate the effect of crack and acoustic emission evolution behaviour during the deformation and damage of rock specimens under the action of SCA, static crushing tests were systematically carried out on tuff specimens in the laboratory. Based on AE real-time monitoring techniques and macroscopic crack observations, the crack evolution mechanism of the cracked specimens during deformation and damage was investigated. The results show that there are three stages of microcrack incubation, macroscopic crack extension and cracking damage during SCA crushing. The tensile stress is 0.06-0.1 times of the compressive stress when brittle materials such as rocks are subjected to SCA leading to cracking damage. A large number of AE events with small amplitudes and a small number of AE events with large amplitudes represent that macroscopic cracks are generated by the rapid aggregation of a large number of microcracks before they are slowly formed. The cracking is usually done by first connecting adjacent holes into lines and then extending to the free surface. The direction of static crushing and the cracking effect can be controlled by designing the borehole location and free surface distribution.*

Keywords: *SCA, Acoustic emission, Crack extension, Expansion pressure, Free surface*

1. Introduction

Static crushing technology is a technique that uses the expansion pressure generated by a static crushing agent (SCA) to load and destroy brittle materials from within. Conventional explosive blasting and mechanical crushing, by applying instantaneous high pressure to the crushed material, causes the material to fail, but also causes the surrounding medium to suffer strong damage. SCA is an expanding cementitious material, the main component of which forms crystals that multiply the volume of the solid phase during the hydration reaction. When the tensile stress (σ_θ) exceeds the ultimate tensile strength, the object cracks, and under continuous expansion pressure, the cracks expand until the brittle material disintegrates and breaks down.

Brittle material components such as rocks can undergo "low stress brittle fracture" at conditions well below fracture damage, demonstrating the presence of cracking effects prior to fracture damage. According to the theory of fracture mechanics[1] Antinao et al.[2] Experimental and numerical studies on fracture toughness and damage mechanisms of rocks under confinement were carried out.

The acoustic emission phenomenon is caused by elastic stress waves generated during rock fracture or deformation within the rock[3] AE technology is used to study the mechanism and characteristics of micro-damage within a material through highly sensitive real-time crack generation monitoring.[4-11] AE sensors capture acoustic signals and analyse them through data acquisition to obtain the location of the source of cracks within the material.[12-15] In this study, Xu et al.[16] quantified the extent of damage within the material by AE energy signatures. dai et al.[17] applied an acoustic emission (AE) system to study and analyse the distribution characteristics of the fracture process zone (FPZ) in Berea sandstone in a three-point bending test. Zhao et al.[18] completed a study of 2D and 3D non-parallel defects on the uniaxial compression damage characteristics of brittle class rocks and investigated the acoustic emission characteristics using a numerical technique correlation method.

ISSN 2663-1563 Vol. 5, Issue 2: 1-9, DOI: 10.25236/AJAGE.2023.050201

Many experiments have been carried out to characterise the variation of acoustic emission parameters and experimental analysis of uniaxial tensile and compressive loading of materials such as rock and concrete. However, there are few studies on the characteristics of AE parameter changes and crack evolution mechanisms during deformation and damage of rocks under the action of SCA. In this study, the variation of expansion pressure and crack evolution characteristics of tuff specimens during static crushing were investigated with the aid of acoustic emission (AE) and experimental macroscopic crack extension analysis. The time-frequency parameter characteristics of the AE technique were used to obtain the evolution of microcracks and the expansion characteristics of macroscopic cracks at different stages within the specimens. This study provides a theoretical basis for the design of SCA for crushing in rock engineering.

2. Pilot study

2.1. Specimen and static crushing design

Natural rocks are usually not ideal linear elastic materials. During static crushing, rocks are subjected to tensile stresses perpendicular to the crack surface, which manifests as Type I damage appearing as the Fracture Process Zone (PFZ), while the plane strain state is more likely to produce critical extension of cracks than the plane stress state. Therefore, it is of great theoretical and practical significance to study the cracking mechanism of static rock crushing. In this study, limestone from the deep foundation pit project of Baiyun Cultural Subway Station of Guangzhou Metro Line 12 was used (Figure 1). It is off-white and flesh-red in its natural state, with a homogeneous texture, an average density of 2.75 g/cm^3, a relatively low degree of weathering and no visible defects on the surface. The material has a uniaxial compressive strength of 82 MPa, a tensile strength of 11 MPa, an internal cohesion of 10.55 MPa, an internal friction angle of 45.8°, a modulus of elasticity of 31-41 GPa, a Poisson's ratio of 0.27, a softening coefficient of 0.73 and a longitudinal wave speed of 3866-4315 m.s.$^{-1}$. The main mineral composition contains calcite (61%), dolomite (23%), clay minerals (15%)), clay minerals (15%) and others. In order to minimise the dispersion of physical parameters and test data from the limestone samples, all rock specimens were taken from the same limestone body. A total of three limestone specimens of 400mm*300mm*300mm were prepared for the test, with the rock sample parameters shown in Table.1 The parameters of the samples are shown in Table 1.

Table 1: for limestone specimens.

No.	Length $l(mm)$	Width $b(mm)$	Height $h(mm)$	Wave speed $V_p(m.s^{-1})$	Weight $m(kg)$
S1	398.20	298.75	299.91	4235	98.11
S2	392.97	298.36	299.95	4197	96.71
S3	399.01	295.85	299.87	3870	97.35

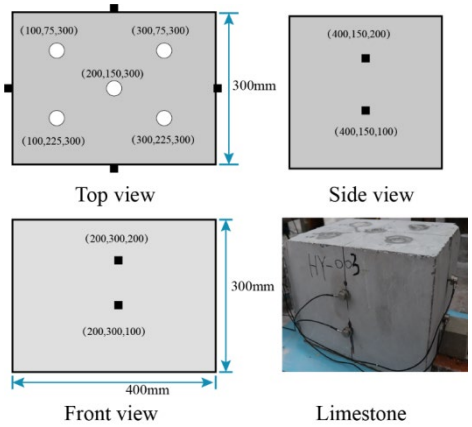

Figure 1: Rock sample size, SCA grout hole design and AE sensor location.

The static crushing agent (Soundless Cracking Agent, SCA) selected for this test was manufactured by the Shanghang County Soundless Cracking Agent Factory, with reference to the standard "Soundless Cracking Agent - JC506-2008". The main components were calcium oxide (81.36%), silica (4.48%), magnesium oxide (3.6%) and other trace elements, as measured by semi-quantitative analysis of fluorescence spectra. The main parameters of the static crushing test were 30mm hole diameter, 0.8H

ISSN 2663-1563 Vol. 5, Issue 2: 1-9, DOI: 10.25236/AJAGE.2023.050201

hole depth, 5 filling holes, 0.3 water to ash ratio, 28°C ambient temperature and 80% air humidity (specimen size and SCA filling hole locations are shown in Figure 1).

2.2. Acoustic emission systems and their principles

Rock specimens are subjected to sustained swelling pressures in the SCA where the material develops micro and macro cracks, resulting in elastic stress waves. The acoustic emission system captures the acoustic signal through a sensor probe, transmits it to the acoustic acquisition system and analyses the energy dissipation, arrival pick-up and source coordinates to determine the spatial location information and evolutionary characteristics of the microcracks in the specimen. The study of the spatial distribution and evolutionary characteristics of the acoustic emission source is based on the algorithmic optimisation of the simplex formed by a swarm of particles. The function relationship between the vertices of each sensor source is first constructed, and the extreme value of the function is obtained through the mathematical model, representing the current optimal and worst solutions respectively. The above steps are repeated in a cycle so that the value of the function approaches the minima point to obtain the acoustic emission location point. The acoustic signal captured by a single sensor probe is called AE impact, and the same signal received per unit time by multiple sensors with different spatial distribution is called AE event.

Figure 2 shows the acoustic emission device for the SCA fractured tuff test. In this experiment, SCA-I was used as the pressure source for rock loading and the Acoustic Emission (AE) system of Beijing Solid Island Technology Co. to effectively receive AE signals from different locations during rock deformation and damage. The main parameters collected during the experiment included hit counts, events, counts, energy, spatial position, amplitude and pick-up time. To filter out ambient noise, the AE device was grounded and the trigger threshold was set at 35 dB. The AE sensor probe was sampled at 3 MHz and the contact surface of the specimen and the AE sensor were coated with petroleum jelly as a coupling agent to ensure a tight fit. The preamplifier gain was set to 40 dB and a lead break test was performed prior to each test to measure the rock wave velocity (VP) and to calibrate the position of the AE sensor.

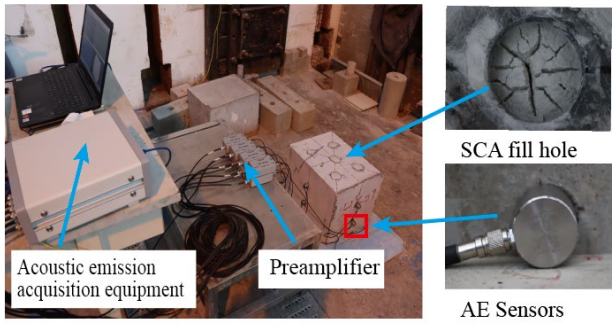

Figure 2: Schematic diagram of the test setup.

2.3. Test procedure

The experimental steps were as follows.

(1) Pre-test preparation. Pre-drilled holes through a rhinestone to a depth of 0.8 of the height of the rock sample, weighed with 1.8kg of SCA and an appropriate amount of distilled water.[19]

(2) Commissioning the AE equipment. The 8 transducer probes of the AE equipment were arranged on the 4 sides of the rock sample, connected to the preamplifier (gain set to 40 dB), then connected to the waveform collector and computer, the earth wire was fixed to a large stable instrument to discharge the interference of ambient noise, and the longitudinal velocity of the material was measured by the lead break test Vp.

(3) Commission the DIC equipment. Choose a high resolution camera, adjust the height and position of the tripod mount, access the computer and debug the brightness of the LED lights to make the captured images high definition and bright.

(4) Fill SCA mix uniform static crusher slurry according to the design ratio and fill into the reserved holes in sequence, record the loading time and turn on the DIC and AE monitoring equipment at the same

ISSN 2663-1563 Vol. 5, Issue 2: 1-9, DOI: 10.25236/AJAGE.2023.050201

time.

(5) Data recording and analysis. Complete data recording of the crack evolution of the chert specimens under SCA crushing, and analysis and processing of the waveform data

3. Test results and AE positioning

The incubation and extension of microcracks (FPZ) during static fracture of rock samples consumes energy of different magnitudes, depending on their size and location.[12]. This dissipated energy is captured by AE sensors, which provide us with information on the evolutionary characteristics of the internal fractures in the form of acoustic signals. It can be observed from the tests that the AE event rates for all rock samples show a similar trend, with microcracks progressively clustering within the material to form macrocracks, and macrocracks expanding in the material medium leading to cracking and damage to the specimen.

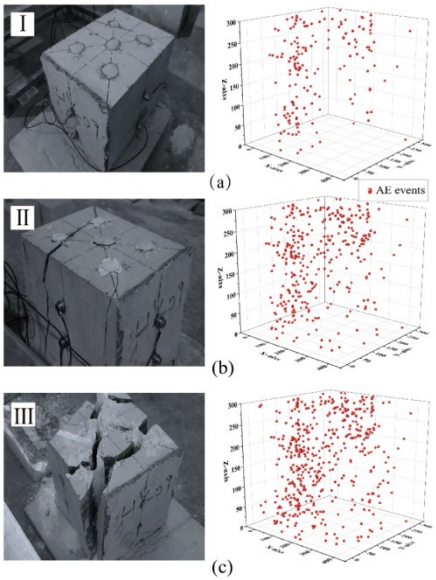

(a) Phase 1, (b) Phase 2, (c) Phase 3.

Figure 3: Macroscopic fractures and AE source localization during SCA crushing of chert specimens.

Comparing the spatial distribution of acoustic emission sources and the distribution characteristics of macroscopic cracks on the surface of the specimen during the damage process of static crushing agent (SCA) loading on rock specimens, the cracking and damage process of rock specimens under the action of SCA expansion pressure can be divided into three stages.

(1) Microfracture gestation stage. Figure 3(a) shows that AE events slowly increase during the microcrack incubation stage, where the AE event localisation rate accounts for 12% of the total event localisation rate, and the expansion pressure in the SCA-filled hole increases from 0 to P. The joints and gaps within the rock material are the first to reach an unstable state after being loaded, leading to the formation of microcracks.

(2) The extension stage of microcracking, also known as the expansion pressure transfer stage. Figure 3(b) represents a significant increase in AE events, as the microcracks agglomerate to form macroscopic cracks, the energy stored within the specimen is released at a faster rate and the impact on the internal particles of the material is further enhanced, contributing to a significant increase in the incidence of AE events.

(3) Rock cracking damage stage. Figure 3(c) figure out the surface macroscopic crack expands to the free surface, the crack width reaches 30mm, the fissures are mutual, fused and penetrated, the specimen is drastically changed internally, this is the peak of AE events, accounting for 62% of the total events, and the specimen is rapidly deformed until it is completely destroyed, accompanied by the sound of cracking inside the specimen.

ISSN 2663-1563 Vol. 5, Issue 2: 1-9, DOI: 10.25236/AJAGE.2023.050201

4. Analysis and discussion

4.1. SCA crushing mechanism

In the borehole of the crushed tuff rock sample, after filling with SCA slurry, as shown in Figure 4 As shown in Figure 4, the SCA hydration reaction under time produces an expansion pressure on the borehole wall, and the crushed body is compressively deformed. At the same time, tensile deformation occurs in the direction perpendicular to the compressive deformation, and when it exceeds the inherent tensile fracture deformation of the crushed body, a fracture process zone (FPZ) of the rock is generated.

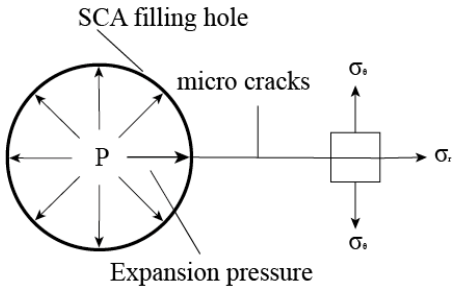

Figure 4: Schematic diagram of microcrack generation.

At the same time, the creation of cracks in the crushed material corresponds to a reduction in the expansion pressure in the hole, but as the static crushing process continues, the rate and width of crack expansion will increase with time. The damage zone is followed by a number of microcracks. The largest of the microcracks expands and causes cracking and crack extension. This is largely dependent on the crack expansion conditions.

From the theory of fracture mechanics[20], the stress intensity factor for a cracked hole wall subjected to expansion forces (K_{IC}) is obtained.

$$K_{IC} = FP\sqrt{\pi a} \tag{1}$$

Where, a - the crack length, i.e. the distance from the centre of the hole to the tip of the crack; R - the radius of the reserved hole.

When a/R = 1 to 1.4, F = 0.1 to 0.34, so the conditions for macroscopic crack expansion are

$$FP\sqrt{\pi a} \geq K_{IC} \tag{2}$$

According to equation (1.9), the expansion pressure required for crack expansion is

$$P_{ex} \geq \frac{K_{IC}}{F\sqrt{\pi a}} \tag{3}$$

Combining the crack evolution characteristics detected by AE and Figure 5 the relationship between the expansion pressure and time in Figure 5, the strength factor of the chert specimens can be calculated from 0.6 to 1.5 by the above equation.

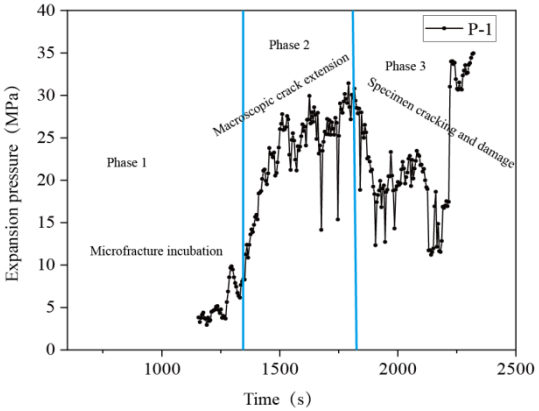

Figure 5: Expansion pressure as a function of time.

ISSN 2663-1563 Vol. 5, Issue 2: 1-9, DOI: 10.25236/AJAGE.2023.050201

The swelling pressure generated by the hydration reaction of the static crushing agent in the hole increases from 0 to P. Local stress concentrations are generated in the hole wall and the specimen receives radial compressive stress σ_r and tangential tensile stress σ_θ internally, resulting in crushing and cracking when the stress limit value is reached. A small area of plastic deformation under the tensile stress σ_θ is called a microcrack (FPZ). The total incidence of AE events is 0.6% when the expansion pressure is increased from 0 to P The surface displacement map through point B shows a slight increase in crack length near the tip of the notch, and given the inhomogeneity within the rock mass, the expansion within the specimen is expected to be less than the calculated P_{ex}.

4.2. AE energy and crack evolution

Figure 6 shows the detailed information between AE impact number, energy and pick-up time for all channels in the three stages of crack evolution for the chert specimens. In this paper, the AE impact number and its energy distribution characteristics are used to investigate the characteristics of microcrack gestation during SCA crushing.

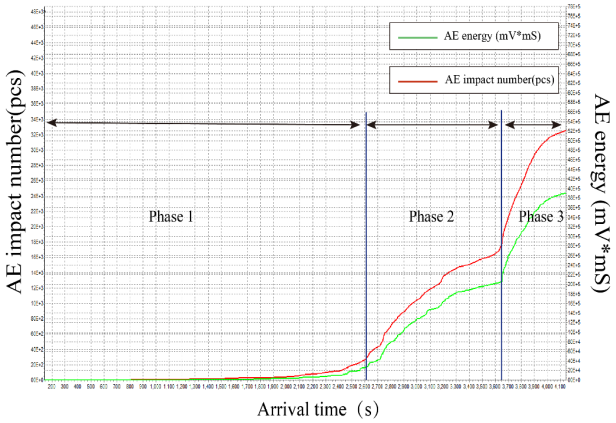

*Figure 6: AE impact number & energy (mV*mS) versus arrival time as a line graph.*

Figure 6 Phase-1 corresponds to the initial stage of the SCA hydration reaction where P increases slowly from 0, loading the rock sample through the pore wall, where elastic deformation occurs within the material and energy is stored, giving rise to microcracking.

Figure 6 Phase-2 corresponds to the continuous hydration reaction of the SCA during static crushing, the swelling pressure gradually increases, the local stress in the reserved hole increases, and the swelling pressure transmits swelling pressure to the rock outside the damage zone using the fracture process zone (FPZ) as a medium. At this point the AE energy is 42% of the total energy corresponding to 40% of the peak expansion pressure P. The number of microcracks increases, which corresponds to an increase in macroscopic cracks on the surface of the specimen. This indicates that at this stage, after the peak of P, the microcracks formed in the rock sample by incubation gather and merge into macroscopic cracks.

Figure 6 Phase-3 corresponds to the point at which the expansion pressure is transmitted through the rock to the vicinity of the free face, with cracks close to the free face expanding first to reach the free face, causing visible cracks to appear in the chert sample until the rock breaks down. At this stage the expansion pressure P rapidly peaks and then decreases to 14% of the peak, the microcrack density increases significantly and the macroscopic crack depth extends to the vicinity of the free surface. This stage indicates that a large number of microcracks are clustered around the fracture process zone (FPZ) and develop into macroscopic cracks extending from the medium to the free surface.

4.3. Drill hole location and crack distribution characteristics

From Figure 7(a) the distribution characteristics of the AE source locations in the X-Y plane can be seen, showing a local aggregation effect, and the area of AE event aggregation shows great correlation with the location of the borehole in the rock specimen and the extension of the macroscopic cracks. The macroscopic cracks on the surface of the chert specimen S1 show a tensile damage pattern as shown in Figure 4. The damage pattern is generally consistent with the spatial distribution characteristics of AE event localisation, with the acoustic emission sources mainly distributed in the tensile zone around the free surface of the specimen. The distribution of the acoustic emission sources is relatively concentrated and the rock fracture zone can be identified by the spatial distribution characteristics of AE event

ISSN 2663-1563 Vol. 5, Issue 2: 1-9, DOI: 10.25236/AJAGE.2023.050201

localisation.

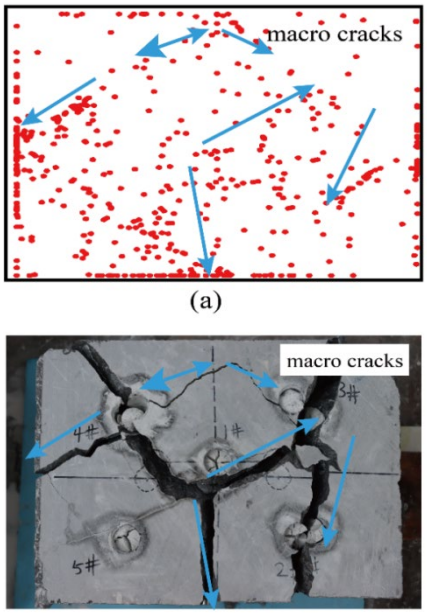

(a) AE event distribution characteristics in the X-Y plane (b) Borehole location and macroscopic crack extension direction.

Figure 7: Macroscopic crack evolution under AE features.

Figure 7(b) figure out the macroscopic crack shape distribution characteristics of the rock sample surface do not exactly match the intensity of AE localisation. As brittle materials produce cracks and fracture process zones (FPZ) during failure, the acoustic emission signal decays rapidly as it propagates through the medium, making it difficult for the same AE event to be collected by multiple sensors simultaneously. Because of the discrepancy between the AE localisation characteristics and the macroscopic crack shape on the surface of the chert specimen, it is difficult for the acoustic emission detection system to accurately quantify the crack generation and extension within the specimen during the damage phase.

Table 2: Crack propagation pattern of hole No. 1 of specimen.

Adjacent holes	Hole spacinga (mm)	Number of cracks (pcs)	Crack shape
2#, 3#	125	4	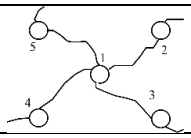
4#, 5#	125	3	

The relationship between crack number, neighboring hole distance, neighboring hole number and free surface of hole No. 1 was analyzed to obtain the crack shape as shown in Table 2. This test used a plum-shaped 5 hole crushing design to analyse and compare the characteristics of the macroscopic crack evolution on the surface. The crack shape around hole 1# in Figure 7(b) and the adjacent holes 2#, 3#, 4# and 5# are connected to each other in a linear pattern. It can be seen that the macroscopic cracks will be the first to produce stress concentration with the adjacent holes as the free surface after formation, thus making the cracking pattern in the static crushing process traceable.

5. Conclusion

The key findings from this pilot study are as follows.

(1) There are three stages in the process of SCA breaking brittle materials, namely the microcrack incubation stage, the macrocrack extension stage and the material cracking stage.

(2) Brittle objects such as rocks exhibit tensile damage under the action of expansion pressure. In actual engineering, the tensile strength of such materials is only 0.06~0.1 times of the compressive

ISSN 2663-1563 Vol. 5, Issue 2: 1-9, DOI: 10.25236/AJAGE.2023.050201

strength, and considering the constraint conditions of the crushed body, SCA with more than 30MPa expansion pressure can be very good for crushing brittle objects such as rocks.

(4) The large number of AE events with small amplitudes and a small number of AE events with large amplitudes during SCA fragmentation represent the fact that macroscopic cracking is only slowly formed by the rapid agglomeration of a large number of microcracks, where energy is continuously stored within the rock and eventually cracked to release energy.

(3) When brittle materials such as rocks are cracked by SCA crushing, the cracks are usually connected into lines first by adjacent holes and then extended to the free surface. In the future, the direction of static crushing and the cracking effect will be controlled by the location of the borehole and the distribution of the free surface in the design process of static crushing.

Acknowledgements

This research work was supported by the Guangzhou Metro Key Areas R&D Program (Item No. HT171787); Guangdong Basic and Applied Basic Research Fund Project (Project No. 2020A1515010560).

References

[1] Xiangji Y, Shiyu L, Ming T. Introduction to rock fracture mechanics [M]. Hefei: University of Science and Technology of China Press, 2010:15-55.
[2] Antinao Fuentealba F J, Bianchi L N, Otegui J L, et al. Accurate experimental determination of rock fracture toughness under simulated reservoir confining pressures[J]. Theoretical and Applied Fracture Mechanics. 2022, 120: 103425.
[3] Keerthana K, Kishen J M C. Micromechanics of fracture and failure in concrete under monotonic and fatigue loadings [J]. Mechanics of Materials. 2020, 148: 103490.
[4] Zhao K, Wang X, Wang L, et al. Investigation of the crack and acoustic emission behavior evolution of red sandstone subjected to water[J]. Theoretical and Applied Fracture Mechanics. 2022, 120: 103419.
[5] Deng H, Yan B, Zhu Y. A new path-independent interaction integral for the SIFs of interfacial crack[J]. Theoretical and Applied Fracture Mechanics. 2022, 120: 103389.
[6] Dong T, Cao P, Lin Q, et al. Fracture evolution of artificial composite rocks containing interface flaws under uniaxial compression[J]. Theoretical and Applied Fracture Mechanics. 2022, 120: 103401.
[7] Han Z, Li D, Li X. Experimental study on the dynamic behavior of sandstone with coplanar elliptical flaws from macro, meso, and micro viewpoints[J]. Theoretical and Applied Fracture Mechanics. 2022, 120: 103400.
[8] Wang G, Wang R, Sun F, et al. Analysis of nonlinear energy evolution in fractured limestone under uniaxial compression [J]. Theoretical and Applied Fracture Mechanics. 2022, 120: 103387.
[9] Wu S, Sun W, Xu X. Study on mode I fracture toughness of rocks using flat-joint model and moment tensor[J]. Theoretical and Applied Fracture Mechanics. 2022, 120: 103403.
[10] Zhao Y, Sun Z, Teng T, et al. Comparative study on modes I and II fracture characteristics of bituminous coal using asymmetric semi-circular bend[J]. Theoretical and Applied Fracture Theoretical and Applied Fracture Mechanics. 2022, 120: 103377.
[11] Zhao Y, Chen C, Qi Q, et al. Rotation and deflection of 3D principal stress axes induced by a prefabricated single flaw in sandstone: A numerical investigation based on DEM[J]. Theoretical and Applied Fracture Mechanics. 2022, 120: 103430.
[12] Arshadnejad S. Design of hole pattern in static rock fracture process due to expansion pressure [J]. International Journal of Rock Mechanics and Mining Sciences. 2019, 123: 104100.
[13] Hasaninia M, Torabi A R. A two-level strategy for simplification of fracture prediction in notched orthotropic samples with nonlinear behavior[J]. Theoretical and Applied Fracture Mechanics. 2022, 120: 103388.
[14] Huang J, Wang H, Zhou L, et al. Analysis of stress intensity factor for a crack emanating from elliptical hole subjected to compressive stress and shear stress[J]. Theoretical and Applied Fracture Mechanics. 2022, 120: 103413.
[15] Jiang Q, Xin J, Xu D, et al. Shear failure process of rectangular tunnel: physical experimental test and numerical back-analysis [J]. Theoretical and Applied Fracture Mechanics. 2022, 120: 103384.
[16] Xu P, Zhou Z, Liu T, et al. In-situ damage assessment of FML joints under uniaxial tension combining with acoustic emission and DIC: Geometric influence on damage formation[J]. Thin-Walled Structures. 2022, 170: 108515.

ISSN 2663-1563 Vol. 5, Issue 2: 1-9, DOI: 10.25236/AJAGE.2023.050201

[17] Dai S, Liu X, Nawnit K. Experimental Study on the Fracture Process Zone Characteristics in Concrete Utilizing DIC and AE Methods [J]. Applied Sciences. 2019, 9(7): 1346.
[18] Zhao Y, Chen C, Wu S, et al. Effects of 2D&3D nonparallel flaws on failure characteristics of brittle rock-like samples under uniaxial compression: Insights from acoustic emission and DIC monitoring[J]. Theoretical and Applied Fracture Mechanics. 2022, 120: 103391.
[19] Lin Q, Wang S, Wan B, et al. Characterization of Fracture Process in Sandstone: A Linear Correspondence Between Acoustic Emission Energy Density and Opening Displacement Gradient[J]. Rock Mechanics and Rock Engineering. 2020, 53(2): 975-981.
[20] Baokun You. Static blasting technology - silent crushing agents and their applications[M]. Beijing: China Building Materials Industry Press, 2008:45-62.